Determination of the Three-Dimensional Structure of Margatoxin by ^{1}H, ^{13}C, ^{15}N Triple-Resonance Nuclear Magnetic Resonance Spectroscopy

Bruce A. Johnson,*,‡ Scott P. Stevens,§ and Joanne M. Williamson§

Department of Biophysical Chemistry and Department of Membrane Biochemistry and Biophysics, Merck Research Laboratories, P.O. Box 2000, Rahway, New Jersey 07065

Received May 31, 1994; Revised Manuscript Received September 28, 1994⊗

ABSTRACT: The solution structure of the 39-residue peptide margatoxin, a scorpion toxin that selectively blocks the voltage-gated potassium-channel $Kv_{1.3}$, has been determined by NMR spectroscopy. The toxin was isotopically labeled with ^{13}C and ^{15}N and studied using two-dimensional homonuclear and three- and four-dimensional heteronuclear NMR spectroscopy. The final structure was determined using 501 constraints, comprising 422 NOE constraints, 60 dihedral angle constraints, 9 disulfide constraints, and 10 hydrogen bond constraints. Structures were initially determined with the program PEGASUS and subsequently refined with X-PLOR. The average rms deviation from a calculated average structure for the backbone atoms of residues 3−38 is 0.40 Å. A helix is present from residues 11 to 20 and includes two proline residues at positions 15 and 16. A loop at residues 21−24 leads into a two-strand antiparallel sheet from residues 25 to 38 with a turn at residues 30−33. Residues 3−6 run adjacent to the 33−38 strand but do not form a canonical β-strand. The two additional residues of margatoxin, relative to the related toxins charybdotoxin and iberiotoxin, insert in a manner that extends the β-sheet by one residue. Otherwise, the global structure is very similar to that of these two other toxins. The longer sheet may have implications for channel selectivity.

Potassium channels are a family of proteins diverse in sequence, biophysical properties, cellular role, and tissue distribution (Hille, 1992). Individual cells may express multiple channel types, complicating the elucidation of their specific roles in modulating cellular function. The investigation of the role of specific types of potassium channels in physiological processes has benefited greatly from the identification of compounds that selectively block a given class of channel. A particularly fruitful source of channel blockers has been the peptide toxins of venoms (Garcia et al., 1991). Several scorpion toxins are known that specifically block potassium channels. The study of one of these toxins, charybdotoxin (Smith et al., 1986; Gimenez-Gallego et al., 1988), has yielded much insight into the nature of toxin−channel interactions and to the characterization of channel properties (MacKinnon & Miller, 1988; Park & Miller, 1992; Stampe et al., 1994).

Charybdotoxin, however, is active against a variety of K^+ channels, including large-conductance Ca^{2+}-activated channels (maxi-K or BK) and some voltage-gated channels ($Kv_{1.3}$) (Vazquez et al., 1989, 1990). This diversity has limited its utility in dissecting channel function in cells exhibiting multiple K^+ channel types. Iberiotoxin, a scorpion toxin with 68% sequence identity to ChTX[1] is selective for maxi-K channels and does not block voltage gated K^+ channels such as $Kv_{1.3}$. Recently, a scorpion toxin with complementary specificity to IbTX has been identified. Margatoxin, isolated from *Centruroides margaritatus* venom, is a 39-residue peptide with 44% sequence identity to ChTX and 41% sequence identity to IbTx (Figure 1), and is selective for $Kv_{1.3}$ (Garcia-Calvo et al., 1993).

These toxins have been particularly useful in dissecting the role of K^+ channels in the process of activation of T lymphocytes. It had been shown previously that charybdotoxin inhibits mitogen-stimulated proliferation of T lymphocytes (Rosa Barros et al., 1989; Grinstein & Smith, 1990; Slaughter et al., 1991). ChTX blocks voltage-gated K^+ channels in T lymphocytes (Price et al., 1989; Sands et al., 1989), and the presence of high affinity binding sites for ChTX in T lymphocytes has been confirmed with binding studies (Deutsch et al., 1991). Both ChTX and high extracellular K^+ decrease IL-2 production and proliferation of lymphocytes, suggesting these effects are mediated by the involvement of K^+ channels in setting membrane potential (Freedman et al., 1992). However, because ChTX is known to be active against both K_v and K_{Ca} channels, the relative role of these two channel types in the antiproliferative effect was unclear. Studies with margatoxin, which blocks the lymphocyte K_v channel but has no effect on lymphocyte K_{Ca} channels, have confirmed the role of the voltage-gated K^+ channel in controlling lymphocyte membrane potential (Leonard et al., 1992). Further studies have demonstrated that MgTX and noxiustoxin (a related $Kv_{1.3}$ blocking toxin) inhibit T lymphocyte proliferation and lymphokine production (Lin et al., 1993), thus identifying $Kv_{1.3}$ as a potential target for novel immunosuppressants.

Understanding the structural basis for MgTX selectivity for $Kv_{1.3}$ may aid in the design of small molecule mimetics of MgTX. Analysis of the effects of specific changes in the toxin sequences may elucidate the role of specific

* To whom correspondence should be addressed.
‡ Department of Biophysical Chemistry.
§ Department of Membrane Biochemistry and Biophysics.
⊗ Abstract published in *Advance ACS Abstracts,* November 1, 1994.
[1] Abbreviations: 2D, 3D, and 4D, two, three, and four dimensional, respectively; ChTX, charybdotoxin; IbTX, iberiotoxin; MgTX, margatoxin. NOE, nuclear Overhauser effect; NOESY, NOESY spectroscopy; TOCSY, total correlation spectroscopy.

0006-2960/94/0433-15061$04.50/0

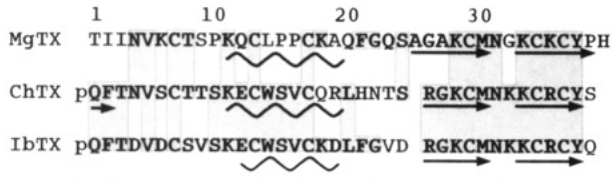

FIGURE 1: Structure based amino acid sequence alignments of MgTX, ChTX, and IbTX. Identical residues are boxed. The first residue of ChTX and IbTX is pyroglutamine. The regions of β-sheet are denoted with a straight arrows and the helical regions with squiggly lines.

residues in toxin−channel interactions. These mutations are best understood in the light of the three-dimensional structure of the toxin. The three-dimensional structures of both ChTX (Bontems et al., 1991a,b, 1992) and IbTX (Johnson & Sugg, 1992) have been elucidated by 2D ^{1}H NMR spectroscopy. The structures of these two toxins are very similar, consisting of an antiparallel β-sheet lying across a helix. Given the sequence homology of MgTX to both ChTX and IbTx, MgTX may show a similar global fold. However, MgTX has some key sequence differences from ChTX and IbTX that may affect its global 3D structure. In particular, it differs from ChTX and IbTX in the insertion of four proline residues, two in the region analogous to the helix of ChTX, and perhaps more importantly, in the presence of two additional residues. We report here the structure of MgTX as determined by NMR spectroscopy. As we had access to a bacterial expression system for MgTX, we were able to perform these studies by two-, three- and four-dimensional NMR of ^{13}C,^{15}N-labeled toxin.

MATERIALS AND METHODS

Materials. 99 atom % NH_4Cl (Isotec); 99 atom % [U-^{13}C]-glucose (Isotec), 98% atom % ^{13}C,^{15}N-CELTONE (Martek); ampicillin, PMSF, and lysozyme were from Sigma; IPTG (Promega); Ni-NTA-agarose (Qiagen); factor X_a, Coomassie Plus protein determination reagent, bovine serum albumin, and trifluoroacetic acid (sequencing grade) were from Pierce; Gradient Ready Gels (4−20%) were from Bio-Rad; HR 10/10 Mono S FPLC column was from Pharmacia; C18 reverse-phase protein and peptide column (1 × 25 cm) was from Vydac. Restriction enzymes were purchased from Life Technologies, Inc.; T4 DNA ligase was from New England Biolabs. Sequenase Version 2.0 DNA sequencing kit was purchased from United States Biochemical; ^{35}Sequetide was from Dupont-New England Nuclear. PCR reagents were from Perkin Elmer Cetus, Inc. Synthetic oligonucleotides were made with an ABI Model 391 DNA synthesizer; reagents were from Applied Biosystems, Inc. Nusieve GTG agarose was purchased from FMC Bioproducts.

Bacterial Strains and Plasmids. Escherichia coli DH5a was used for plasmid propagation. *E. coli* BL21(DE3) was used for expression of the fusion protein (Studier & Moffat, 1986). Plasmid, pMGTX, has been described previously (Garcia-Calvo et al., 1993).

Cloning Methods. p6HISMGTX was constructed as follows: Polymerase chain reaction was performed with pMGTX (100 ng) as template and oligonucleotides 5′-TCGACGGATCCCATCACCATCACCATCACG-GGATCTGTCGACGGATCTATCGAAGGTC-3′ and 5′-TCGATAAGCTTCCTATCAGTGCGGGTAGC-3′ to generate a DNA fragment that incorporated six histidine residues between the fusion protein and the factor X_a cleavage site. The resulting PCR product was phenol/chloroform extracted, ethanol precipitated, restriction digested, gel purified on 3% Nusieve agarose, and ligated into pMGTX by standard techniques (Ausubel et al., 1989). Placement of the six histidines was verified by dideoxy sequencing with Sequenase (Sanger et al., 1977).

Purification of MgTX. The growth medium contained (in g/L of distilled, deionized water): $Na_2HPO_4{\cdot}7H_2O$ (12.8), KH_2PO_4 (3.0), NaCl (0.5), 99 atom % $^{15}NH_4Cl$ (1.0), $MgSO_4$ (0.24), $CaCl_2$ (0.01), 99 atom % [U-^{13}C]glucose (1.9), 98 atom % ^{13}C,^{15}N-CELTONE (0.9), and ampicillin (0.2). Each liter of medium was inoculated with a single colony of BL21-(DE3)/p6HISMGTX. A total of 6 L of medium was inoculated. When the A_{650nm} had reached 0.7−0.8 (after about 11 h of incubation at 37 °C and 250 rpm), IPTG was added to each liter of culture at a final concentration of 0.5 mM along with additional ampicillin (0.1 g). Incubation was continued as before for 3 h after IPTG addition. The cells were harvested by centrifugation, washed once with buffer A (400 mL; 50 mM sodium phosphate, 300 mM sodium chloride, pH 8.0), and frozen in liquid N_2.

All purification steps were carried out at 4 °C unless otherwise specified. The cells were thawed in buffer A (60 mL) also containing 1 mM PMSF and 10 mM β-mercaptoethanol lysed by a combination of lysozyme treatment and sonication as described previously (Park et al., 1991). The extract was clarified by centrifugation at 28000*g* for 1 h. The supernatant solution was loaded onto a column (bed volume = 125 mL) of Ni-NTA agarose equilibrated in buffer A. The column was washed with buffer A (500 mL), followed by 500 mL of a buffer containing 50 mM sodium phosphate, 300 mM sodium chloride, and 5 mM imidazole, pH 7.0. These washes were discarded. The fusion protein was eluted from the resin with a buffer containing 50 mM sodium phosphate, 300 mM sodium chloride, and 100 mM imidazole, pH 7.0. Fractions (8 mL) were collected and analyzed by SDS−PAGE on 4−20% gradient gels for the presence of the fusion protein. Fractions (9−19) were combined and concentrated by addition of solid $(NH_4)_2SO_4$ to 50% of saturation. The precipitate was collected by centrifugation and dissolved in a minimum volume of 50 mM Tris-HCl, 150 mM sodium chloride, and 0.5 mM β-mercaptoethanol, pH 8.3 buffer. This solution was dialyzed against the same buffer (three changes of 2 L each) overnight. The protein concentration of the dialyzed solution was determined by the Coomassie blue method (Sedmark & Grossberg, 1977) with bovine serum albumin as standard. After affinity purification and dialysis, 560 mg (V_t = 25 mL) of fusion protein were isolated. Factor X_a (0.5 mg; 72 units) and $CaCl_2$ (5 mM) were added to the dialyzed solution. It was incubated at room temperature for 18 h. The progress of fusion protein cleavage was monitored by SDS−PAGE as described previously. Following cleavage from the fusion protein, MgTX was purified by ion exchange and C18 reverse-phase chromatographies as described previously (Garcia-Calvo et al., 1993). The final yield of ^{13}C,^{15}N-MgTX was 13 mg as estimated by measurement of A_{235nm} (Garcia-Calvo et al., 1993). The sample was dissolved in a solution of 50 mM sodium acetate at pH 4.6 with a protein concentration of 2.4 mM. Two pairs of samples were used: unlabeled protein and ^{13}C,^{15}N-labeled protein, each in 99.99% D_2O and in 90% H_2O/10% D_2O.

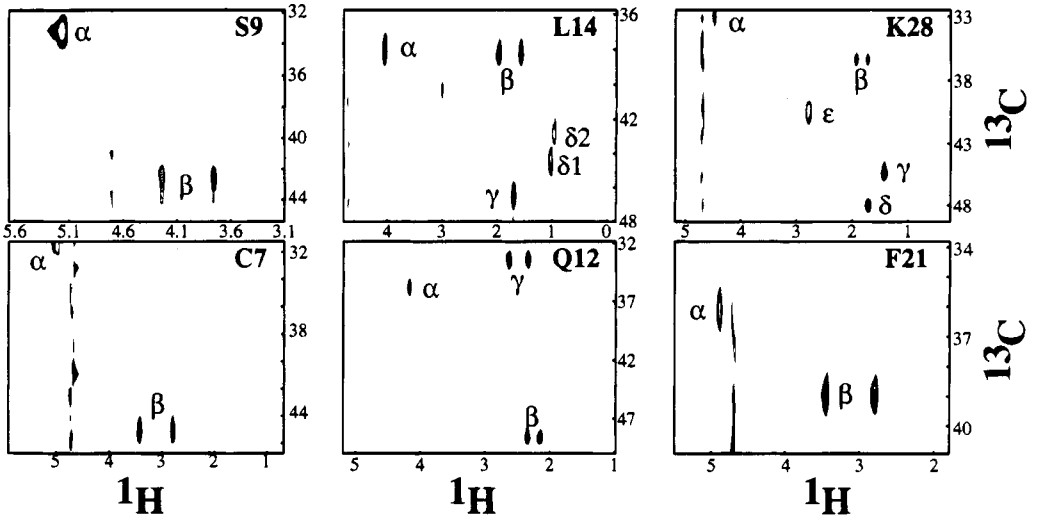

FIGURE 2: Contour plots of the 4D HCACH-TOCSY experiment chosen at six different pairs of $^{1}H_{\alpha}-^{13}C$ chemical shifts coinciding with the positions of residues C7, S9, Q12, L14, F21, and K28. The cross peaks are labeled according to the corresponding carbon. The sweep width for the ^{13}C dimension is less than the total ^{13}C chemical shift range so some peaks are folded by an integer multiple of the sweep width from their true position.

NMR Spectroscopy. All NMR measurements were performed on either a Varian Unity 500 spectrometer with three RF channels or a Unity Plus 600 spectrometer with four RF channels. All experiments were acquired with quadrature detection in the indirectly detected dimensions using the TPPI−States method (Marion et al., 1989).

The following heteronuclear NMR spectra were acquired: 4D HCA(CO)NNH and HCANNH (Boucher et al., 1992), 4D TOCSY-HCACH (Johnson, unpublished results), 4D $^{13}C,^{15}N$-edited NOESY (Kay et al., 1990), 4D $^{13}C,^{13}C$-edited NOESY, 3D CT-HCACO (undecoupled), (Powers et al., 1991; Vuister et al., 1992), 2D HNCA (Schmieder et al., 1991), and 3D HN(CO)HB (Grzesiek et al., 1992).

The sweep widths, acquired data size (complex), processed data size, carrier position, and mixing times were as follows: HCA(CO)NNH, 1800 Hz ($^{1}H\alpha$, t_1), 1600 Hz ($^{13}C\alpha$, t_2), 1200 Hz (^{15}N, t_3), and 6000 Hz (^{1}HN, t_4), 32 × 8 × 8 × 512, 64 × 32 × 32 × 512, 4.73 ppm; HCANNH, 1800 Hz ($^{1}H\alpha$, t_1), 1600 Hz ($^{13}C\alpha$, t_2), 1200 Hz (^{15}N, t_3), and 4500 Hz (^{1}HN t_4), 32 × 8 × 8 × 320, 64 × 32 × 32 × 512, 8.3 ppm; $^{13}C,^{15}N$-edited NOESY, 4000 Hz (^{1}H, t_1), 2600 Hz (^{13}C, t_2), 1200 Hz (^{15}N, t_3), and 5000 Hz (^{1}HN, t_4), 32 × 8 × 8 × 1024, 64 × 32 × 32 × 512, 8.3 ppm, 200 ms; HCACH-TOCSY, 1800 Hz ($^{1}H\alpha$, t_1), 1600 Hz ($^{13}C\alpha$, t_2), 2600 Hz (^{13}C, t_3), and 5000 Hz (^{1}H, t_4), 32 × 8 × 12 × 256, 64 × 32 × 32 × 512, 3.0 ppm, 24 ms; $^{13}C,^{13}C$-edited NOESY, 2600 Hz (^{13}C, t_1), 3000 Hz (^{1}H, t_2), 2600 Hz (^{13}C, t_3), and 4500 Hz (^{1}H), 8 × 64 × 8 × 128, 32 × 128 × 32 × 256, 3.0 ppm, 200 ms; CT-HCACO, 5000 Hz ($^{13}C\alpha$, t_1), 1875 Hz (^{13}CO, t_2), and 2800 Hz (^{1}H, t_3), 32 × 32 × 512, 64 × 64 × 512, 4.73 ppm; HN(CO)HB, 2600 Hz (^{15}N, t_1), 6000 Hz (^{1}H, t_2), 6499 (^{1}H, t_3), 32 × 64 × 512, 64 × 128 × 512; HNHA, 3000 Hz (^{13}C, t_1) and 6499 Hz (^{1}H, t_2), 512 × 1024, 1024 × 1024, 8.3.

The ^{13}C and ^{15}N dimensions of the HCA(CO)NNH, HCANNH, $^{13}C,^{15}N$-edited NOESY, HCACH-TOCSY, and the $^{13}C,^{13}C$-edited NOESY were extended with complex linear prediction prior to the Fourier transform. The non-signal containing regions of the directly detected dimensions were discarded after the first FT when appropriate.

In addition to the above heteronuclear experiments, 2D TOCSY (Braunschweiler & Ernst, 1983; Davis & Bax, 1985) with mixing times from 16 to 84 ms, 2D NOESY (Jeener et al., 1979; Macura e al., 1981) spectra with mixing times from 50 to 200 ms, 2D ROESY (Bothner-By et al., 1984; Bax & Davis, 1985) with a mixing time of 80 ms, and 2D ECOSY (Griesinger et al., 1982) spectra were acquired.

The rate of exchange of amide protons with solvent deuterons was determined qualitatively by following the disappearance of amide proton peaks from 1D spectra and 2D NOESY spectra. A sample lyophilized from 90% H_2O was dissolved in 99.99% D_2O and 1D single-pulse and 2D NOESY spectra were taken as previously described (Johnson & Sugg, 1992).

Spectra were processed with a version of FELIX (Biosym, Inc.) modified to include complex linear prediction (Barkhuijsen et al., 1985; Johnson, unpublished results), water-suppression processing (Johnson, 1992), and improved baseline correction capabilities. Spectra acquired in $^{1}H_2O$ with detection of amide protons were processed with the APSB method (Johnson, 1992) to eliminate the dispersive signal from residual water. All spectral display and analysis was done with the program NMRView (Johnson & Blevins, 1994).

Structure Determination. The disulfide bonding pattern was initially obtained using NMR methods similar to that used previously for iberiotoxin (Johnson & Sugg, 1992). We generated a set of 100 structures without using any disulfide constraints and analyzed the S^{γ}-S^{γ} distances in the 20 lowest energy structures. The minimum, average, and maximum $S^{\gamma}-S^{\gamma}$ distances among the set of structures was lowest for the three disulfide pairs (7−29, 13−34, and 17−36) which are analogous to those observed in the related toxins iberiotoxin (Johnson & Sugg, 1992) and charybdotoxin (Sugg et al., 1990). Subsequent to this analysis the disulfide bond between Cys^7 and Cys^{29} was confirmed with enzymatic cleavage and amino acid analysis of the resulting fragment (Bednarek et al., 1994).

Structures consistent with the NMR data were determined using the program PEGASUS as previously described (Johnson & Sugg, 1992). Additional refinement of the structures was done using the simulated annealing protocol described in the "refine" script of X-PLOR (Brünger, 1991).

Table 1: ^{1}H, ^{13}C, and ^{15}N Chemical Shift Assignments for Margatoxin at pH 4.6 and 25 °C

Ala	N	HN	Cα	Hα	Cβ	Hβ	C′	Ala	N	HN	Cα	Hα	Cβ	Hβ	C′
19	122.72	8.00	53.14	4.11	16.40	1.47	169.57	27	119.55	8.27	50.13	5.63	23.70	1.25	172.90
25	124.73	7.72	51.92	4.22	18.60	1.35	171.21								

Asn	N	HN	Cα	Hα	Cβ	Hβ	Hδ2	C′
4	124.68	8.71	50.78	4.86	36.31	2.91, 2.65	7.56	174.23
31	125.82	9.45	52.53	4.38	35.81	3.10, 2.77	7.57	173.18

Cys	N	HN	Cα	Hα	Cβ	Hβ	C′	Cys	N	HN	Cα	Hα	Cβ	Hβ	C′
7	116.62	8.01	52.08	4.99	45.13	3.43, 2.80	174.56	29	122.02	8.79	53.92	5.05	38.71	2.79, 2.37	175.19
13	113.89	7.41	51.49	4.69	36.31	2.65, 3.06	173.52	34	121.20	8.56	53.78	5.06	36.41	2.71, 2.72	174.72
17	116.64	7.68	55.23	4.86	33.42	2.98, 2.89	171.45	36	121.91	8.52	49.63	5.45	35.90	2.33, 2.83	174.39

Gln	N	HN	Cα	Hα	Cβ	Hβ	Cγ	Gln	N	HN	Cα	Hα	Cβ	Hβ	Cγ
12	115.03	7.13	56.41	4.17	27.80	2.35, 2.14	33.30	23	116.17	8.50	56.89	3.91	26.99	2.22, 2.12	32.00
20	114.53	7.26	55.95	4.05	28.24	1.82, 1.46	31.70								

Gln	Hγ	Hε2	C′	Gln	Hγ	Hε2	C′
12	2.64, 2.34	7.56	172.14	23	2.50, 2.52	8.35	171.90
20	1.85, 1.52		171.39				

Gly	N	HN	Cα	Hα	Gly	N	HN	Cα	Hα
22	111.62	7.94	42.56	3.96, 4.70	32	127.07	8.12	44.10	4.15, 4.15
26	107.85	8.31	41.41	3.73, 4.56					

His	N	HN	Cα	Hα	Cβ	Hβ	Cδ2	Hδ2
39	122.38	8.01	55.08	4.53	29.16	3.25, 2.94	118.63	7.33

His	Cε1	Hε1	C′
39	134.4	8.46	170.03

Ile	N	HN	Cα	Hα	Cβ	Hβ	Cγ	Hγ1
2	127.04	8.70	58.99	4.46	37.15	1.84	26.19	1.16
3	124.18	8.35	58.79	4.46	38.00	1.95	25.63	1.18

Ile	Cδ1	Hδ1	Cγ	Hγ2	C′
2	11.15	0.89	15.96	0.92	172.88
3	11.94	0.81	16.05	0.94	173.03

Leu	N	HN	Cα	Hα	Cβ	Hβ	Cγ	Hγ
14	121.67	7.35	58.46	4.03	38.04	1.97, 1.61	25.86	1.71

Leu	Cδ	Hδ1	Cδ	Hδ2	C′
14	23.88	1.03	22.05	0.98	173.92

Lys	N	HN	Cα	Hα	Cβ	Hβ	Cγ	Hγ	Lys	N	HN	Cα	Hα	Cβ	Hβ	Cγ	Hγ
6	127.22	8.37	53.70	4.78	32.12	1.66, 1.85	23.36	1.56, 1.45	28	118.02	9.05	53.95	4.49	36.26	1.95, 1.73	24.64	1.43, 1.42
11	117.94	7.95	58.11	4.02	30.66	1.84, 1.85	23.62	1.48, 1.03	33	120.61	7.64	52.68	5.21	34.40	1.76, 1.96	23.53	1.53, 1.46
18	122.45	8.76	56.29	4.61	31.30	1.63, 1.84	24.83	1.61, 1.60	35	124.35	9.10	53.11	4.67	34.01	1.64, 1.77	23.65	1.14, 1.14

Lys	Cδ	Hδ	Cε	Hε	C′	Lys	Cδ	Hδ	Cε	Hε	C′
6	27.68	1.73, 1.65	40.18	3.01, 3.01	173.09	28	27.32	1.72, 1.69	40.40	2.77, 2.78	175.16
11	27.43	1.72, 1.49	40.27	3.02, 2.79	169.12	33	27.50	1.75, 1.71	40.27	3.02, 3.02	172.35
18	28.02	1.64, 1.64	40.87	3.13, 2.95	168.58	35	27.52	1.66, 1.66	40.31	2.99, 2.79	174.28

Met	N	HN	Cα	Hα	Cβ	Hβ
30	128.63	8.92	52.40	4.83	32.52	2.13, 1.83

Met	Cγ	Hγ	C′
30	30.14	2.47, 2.47	173.66

Phe	N	HN	Cα	Hα	Cβ	Hβ	Cδ1	Hδ
21	113.93	8.26	56.53	4.90	38.77	2.79, 3.46	130.37	7.34

Phe	Cε	Hε	Cζ	Hζ	C′
21	129.57	7.19	130.86	7.53	172.82

Table 1 (Continued)

Pro	Cα	Hα	Cβ	Hβ	Cγ	Hγ	Pro	Cα	Hα	Cβ	Hβ	Cγ	Hγ
10	63.80	3.97	30.07	2.08, 2.36	26.37	2.22, 2.21	16	64.38	4.53	28.79	1.86, 2.31	26.34	2.30, 2.16
15	65.72	4.50	27.57	2.02, 2.27	25.77	2.29, 2.09	38	61.52	4.08	30.83	1.85, 2.12	25.38	1.74, 1.26

Pro	Cδ	Hδ	C′	Pro	Cδ	Hδ	C′
10	49.27	4.11, 3.94	170.72	16	48.97	3.91, 3.52	168.73
15	48.60	3.92, 3.51	171.83	38	48.90	3.53, 2.99	173.09

Ser	N	HN	Cα	Hα	Cβ	Hβ	C′
9	119.01	8.10	53.97	5.16	63.45	4.23, 3.76	175.19
24	113.16	8.34	56.29	4.51	61.80	4.05, 3.92	174.46

Thr	N	HN	Cα	Hα	Cβ	Hβ	Cγ2	Hγ2	C′
1			60.08	3.75	68.26	3.84	19.86	1.24	177.46
8	109.29	9.27	60.29	4.41	68.79	4.40	20.29	1.23	174.25

Tyr	N	HN	Cα	Hα	Cβ	Hβ
37	121.04	8.30	53.85	4.62	38.27	2.36, 2.89

Tyr	Cδ1	Hδ	Cε1	Hε	C′
37	131.57	6.91	116.46	6.58	175.63

Val	N	HN	Cα	Hα	Cβ	Hβ
5	122.87	7.99	60.22	4.12	33.84	1.62

Val	Cγ	Hγ1	Cγ	Hγ1	C′
5	19.93	0.92			173.93

Upper bound constraints were determined from the peak volumes in the 2D ^{1}H NOESY and 4D ^{13}C,^{13}C- and ^{13}C,^{15}N-edited NOESY spectra. The spectral peaks were picked using NMRView, and the upper bound constraint was calculated based on the $1/r^6$ dependence of NOE intensity on distance. The constraints were initially calibrated against the distance expected for peaks found in defined regions of secondary structure as previously described for our analysis of iberiotoxin (Johnson, 1992). As constraints were defined from 2D ^{1}H−^{1}H, 4D HCCH, and 4D HNCH NOE spectra the calibration was done individually for each spectrum.

After a set of preliminary structures were determined, the NOEs were interactively calibrated against the corresponding distance in the structures in a manner similar to that described for the program CALIBA (Güntert et al., 1991). This analysis was performed using the program NMRView. NOE and coupling constant measurements were used to obtain torsional restraints for the ϕ, ψ, and χ angles and stereospecific assignments of the β-methylene protons. Intraresidue and sequential distances between NH, C_αH, and C_βH protons were obtained from the NOESY spectrum with 50-ms mixing time. Analysis of the spin-coupling constant, $^3J_{HN\alpha}$, was done by analysis of absorptive and dispersive rows of the DQF-COSY spectrum (Kim & Prestegard, 1989; Johnson & Sugg, 1992) and using a heteronuclear HNCA experiment (Schmieder et al., 1991). The $^3J_{\alpha\beta}$ coupling constants were estimated from the TOCSY spectra (Driscoll et al., 1989) and ECOSY spectra. The spin-coupling constant $^1J_{C\alpha H\alpha}$ was measured from the 3D CT-HCACO spectrum. All values were greater than 134 Hz, indicative of negative ϕ torsion angles (Vuister et al., 1992). The $^3H_\beta$−CO coupling constant was estimated from the HN(CO)HB spectrum (Grzesiek et al., 1992). These constraints were used to derive the torsional restraints and stereospecific assignments by means of a grid search routine in NMRView similar to those previously described (Nilges et al., 1990; Güntert et al., 1991).

RESULTS

Sequential Assignments. The chemical shifts of the backbone atoms of margatoxin were assigned using the combination of the two four-dimensional experiments, HCA-(CO)NNH which provides sequential connectivities and HCANNH which provides intraresidue connectivities. In addition, we observed nearly all of the sequential connectivities in the HCANNH experiment through the two-bond CA_iN_{i+1} connectivity (Boucher et al., 1992). The locations of the cross peaks were determined with the peak-picking routines in NMRView. The two peak lists were then automatically correlated to identify sequentially adjacent residues and form stretches of Gly or Pro bounded residues (Campbell-Burk et al., 1992). Every expected connectivity was observed and these residue sequences were readily placed in their correct location on the basis of their length and presence of Gly or Pro as the stop or start residue. The side-chain resonances were then determined by use of a four-dimensional HCACH-TOCSY experiment. Planes exhibiting the ^{1}H,^{13}C frequencies of this experiment were selected at the ^{1}Ha,^{13}Cα chemical shifts of the desired residue (Figure 2). The overlap of ^{1}Ha,^{13}Ca chemical shifts was generally small enough that these planes contained only cross peaks from a single residue. The residue type was confirmed by the characteristic pattern of chemical shifts. The shifts were entered into the database. The assignments were confirmed by comparing the ^{1}H chemical shifts to those observed in the two-dimensional TOCSY experiments. The side-chain resonances of the aromatic residues were assigned using the two-dimensional TOCSY and 4D NOESY experiments. The chemical shift of the carbonyl carbons was determined using the HCACO experiment. From the results of these experi-

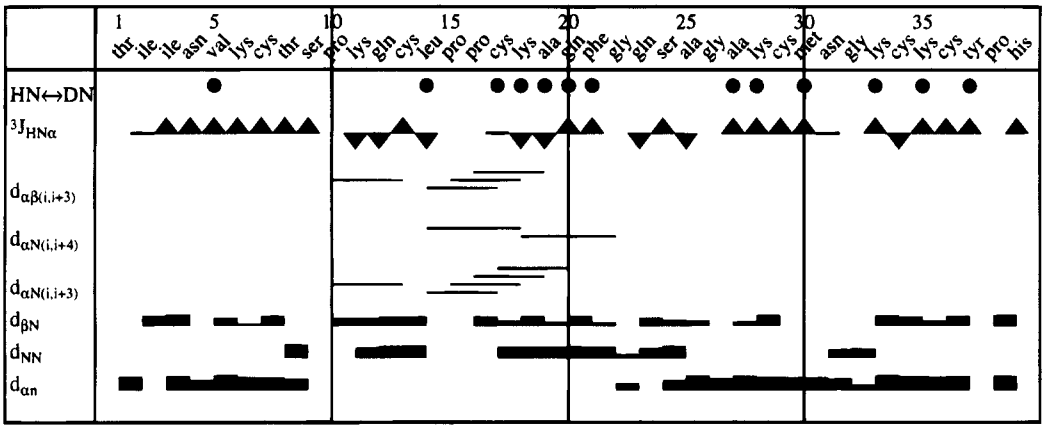

FIGURE 3: Summary of short-range NOEs ($|i - j| < 5$) involving NH, $C^{\alpha}H$, $C^{\beta}H$, $^3J_{HN\alpha}$, and amide proton exchange rates. The height of the lines for sequential NOEs is proportional to the upper distance bound calculated from the NOE intensity. Coupling constants $^3J_{HN\alpha}$ greater than 8 Hz are indicated as (▲) and less than 6 Hz as (▼), and those with values between 6and 8 Hz are indicated as (—). Amide protons persistent in the 1D spectra taken 90 min after exchange in D_2O are indicated as (●).

Table 2: Structural Statistics for Margatoxin

structural statistics	PEGASUS	X-PLOR[a]
number of structures[b]	50	23
rms deviations from experimental distance restraints (Å)		
all NOE (422)	0.057 ± 0.001	0.038 ± 0.001
intraresidue (169)	0.049 ± 0.002	0.044 ± 0.001
interresidue sequential ($\|i - j\| = 1$) (117)	0.059 ± 0.005	0.026 ± 0.007
interresidue short range ($1 < \|i - j\| \leq 5$) (57)	0.077 ± 0.001	0.050 ± 0.002
interresidue long range ($\|i - j\| > 5$) (79)	0.052 ± 0.001	0.022 ± 0.002
bonds (19,10)[c]	0.162 ± 0.014	0.031 ± 0.010
rms deviations from experimental dihedral restraints (deg) (60)	0.196 ± 0.016	0.859 ± 0.161
deviations from idealized covalent geometry[d]		
bonds (Å)	0.0	0.004 ± 0.000
angles (deg)	0.0	0.752 ± 0.015
impropers (Å)	0.0	0.411 ± 0.041
E_{L-J} (kcal mol)[e]	−65 ± 8	−35 ± 5

[a] The X-PLOR structures are the structures originally calculated in PEGASUS and then refined with the simulated annealing protocol. The force constants for the experimental restraints used in the simulated annealing are $F_{NOE} = 50$ and $F_{tor} = 200$. During the simulated annealing run the temperature is reduced from 2000 to 100 K, and F_{rep} is increased from 0.003 to 4.0 kcal mol^{-1} Å^{-4} over 4000 steps. [b] The number of structures for which there were no distance violations greater than 0.4 Å, no bond violations greater than 0.4 Å, and no dihedral angle violations greater than 5°. Only these structures are used for the statistics. [c] In PEGASUS, 10 constraints were used for 5 hydrogen bonds and 9 constraints for 3 disulfide bonds. In X-PLOR the disulfide bonds were included explicitly in the PSF file. [d] PEGASUS is a rigid geometry program so the covalent geometry remains at the canonical values. [e] The PEGASUS refinement includes a final stage of explicit refinement against the van der Waals energy (Robson & Platt, 1986). The X-PLOR refinement is done only with the repel function with a final radius of 0.75 times the standard values used in the CHARMM (Brooks et al., 1983) empirical energy function. E_{L-J} is measured in both cases within PEGASUS.

ments nearly every ^1H, ^{13}C, and ^{15}N resonance was assigned (Table 1).

The secondary structure of margatoxin was derived from the short range NOEs, $^3J_{HNa}$, and deuterium exchange measurements indicated in Figure 3 as well as carbon chemical shifts and long-range NOE measurements. A helix is present from approximately residues 11 to 20. A loop connects the helix to the first strand of the sheet via a half-turn (Wüthrich, 1986). The antiparallel sheet comprises two strands from residues 25 to 38 with a turn at residues 30−33. The amino-terminal residue is disordered. Residues 3−6 run adjacent to the 33−38 strand of the sheet, but the lack of slow deuterium exchange and of strong CαH−CαH NOES is inconsistent with the formation of a true strand of the sheet.

Distance constraints were extracted from both 2D ^1H−^1H, 4D ^1H,^{13}C HCCH and 4D ^1H,^{13}C,^{15}N HNCH NOESY spectra. The final tertiary structure was determined from a total of 422 (169 intraresidue, 117 sequential, 57 short-range, and 79 long-range) NOE-based distance constraints, 60 dihedral angle constraints, 9 disulfide distance constraints (three per bond), and 10 hydrogen bond distance constraints (2 per bond) for residues in the β-sheet. The number of interresidue NOEs is nearly double that obtained in previous studies of the related toxins ChTX (Bontems et al., 1992) and IbTX (Johnson & Sugg, 1992), and this is certainly in part due to the use of the heteronuclear experiments. The structural statistics for the PEGASUS and X-PLOR structures are reported in Table 2. The best fit superpositions of the final 23 structures generated with PEGASUS and refined with X-PLOR are illustrated in Figure 4. As can be seen from the figure, the structures are well defined. Most residues show backbone rms deviations from the average coordinates of less than 0.4 Å. The amino-terminal four residues and the carboxyl-terminal residue, as well as residues at the loop between the helix and sheet and in the turn region at residues 30−31, show greater disorder. The backbone disorder at 30−31 is manifested primarily as two discrete states, the predominant state is that of a type 1 turn. The $^3J_{HNH\alpha}$ coupling for residue 31 is 6.7 Hz, consistent with conformational averaging of the Φ angle. In this small protein most residues have significant surface accessibility,

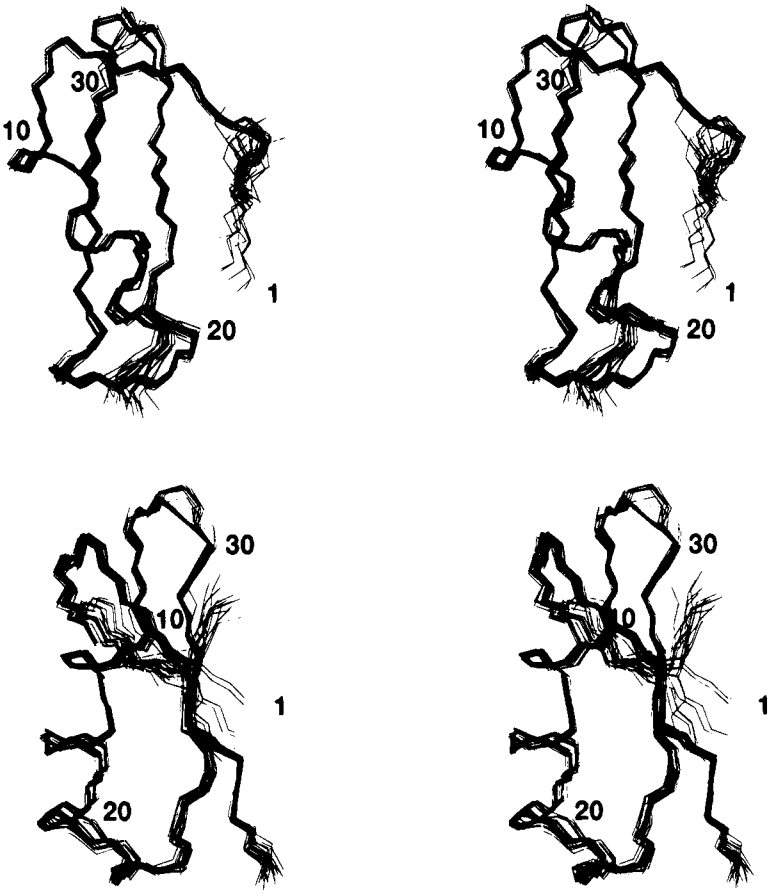

FIGURE 4: Stereodiagrams of the best fit superpositions of the 23 structures generated with PEGASUS and refined with X-PLOR. The two views differ by an approximately 90° rotation about the y axis.

Table 3: Atomic Rms Differences (Å)

	residues 3−38		residues 1−39	
	backbone atoms[a]	all atoms[b]	backbone atoms	all atoms
⟨SA⟩ vs $\overline{\text{SA}}$[c]	0.40	0.84	0.68	1.32
⟨PEG⟩ vs $\overline{\text{PEG}}$	0.60	0.89	0.78	1.37
$\overline{\text{PEG}}$ vs $\overline{\text{SA}}$	0.97	1.42	1.03	1.45

[a] Backbone atoms consist of the atoms N, CA, C, and O. [b] All non-hydrogen atoms. [c] The structures are denoted as follows: ⟨SA⟩, the final stimulated annealing structures; $\overline{\text{SA}}$, the mean structure obtained by averaging the coordinates of the individual SA structures after the best fit superposition; ⟨PEG⟩, the final PEGASUS structures; $\overline{\text{PEG}}$, the mean structure obtained by averaging the coordinates of the individual PEGASUS structures.

and the side chains show correspondingly high levels of disorder. Exceptions to this are, in particular, the Cys residues which are buried in the formation of disulfide bonds forming the core of the protein. Most χ_1 torsion angles are, however, with the exception of residue 11 and those residues in regions with disordered backbones, well defined with rms deviations of less than 20°. The global rms deviations for the structures generated with both PEGASUS and X-PLOR are indicated in Table 3. The structures refined with X-PLOR show approximately 0.2 Å smaller rms deviation of the backbone atoms than do the PEGASUS structures.

DISCUSSION

The overall structure of MgTX is similar to that of ChTX and IbTX. A superposition of MgTX, ChTX, and IbTx is shown in Figure 5. All three toxins consist of a β-sheet with a helix lying across it at approximately a 40° angle. A Cys-X-Cys sequence in N-terminal strand of the sheet is connected to a Cys-X-X-X-Cys sequence in the helix via two disulfide bonds. A third disulfide bond connects the previous strand to the extended strand prior to the helix. In ChTX, the amino terminus of the toxin forms a third strand of the β-sheet. In IbTX, while this strand runs adjacent to the amino-terminal strand of the sheet, the pattern of NH exchange and NOEs was not consistent with the formation of a canonical strand of sheet under the conditions studied (Johnson & Sugg, 1992). The situation is similar in MgTX where this strand shows NOEs to the amino-terminal strand of the sheet and some of the expected NH protons are moderately slow in exchange, but the pattern is not consistent with a well formed strand of sheet. In MgTX, this may in part be due to the presence of a proline at residue 38, whose side chain precludes close contact of the carboxyl-terminal backbone with the amino-terminal backbone.

The sequence of MgTX differs from the other two toxins in having two additional residues. Comparison of the structures of these toxins indicates that these two additional residues insert in a manner which extends the β-sheet by a residue at each end relative to ChTX and IbTX (Figures 1 and 5). In light of the structures the sequence alignment shown in Figure 1 was obtained, which differs in the placement of the insertion from the previously presented sequence alignment (Garcia-Calvo et al., 1993). This alignment is meant to be representative of the structural alignments and not necessarily indicative of the mutational

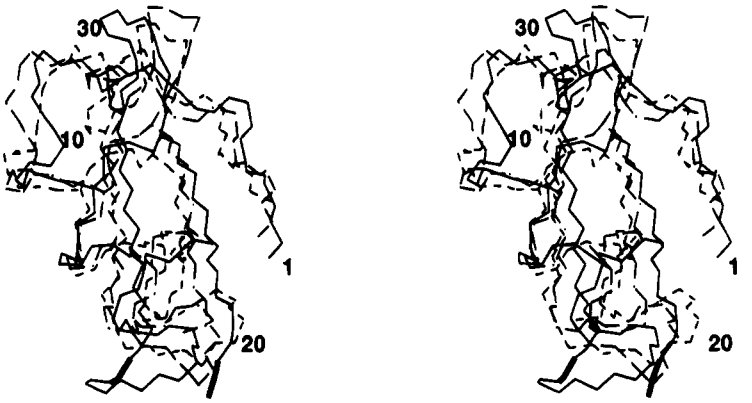

FIGURE 5: Best fit superposition of the NMR-derived structures of MgTX (solid lines), IbTx (short-dashed lines) (Johnson & Sugg, 1992), and ChTX (long-dashed lines) (Bontems et al., 1992). The MgTX structure is the lowest energy structure after the X-PLOR refinement. The ChTX structure displayed is the first structure in the file stored with accession code 2CRD in the Protein Data Bank (Berstein et al., 1977). The backbone atoms (N, CA, C, and O) of the following residues were used for the superposition: 3−20 and 25−36 of ChTX and IbTX, and 3−20 and 26−37 of MgTX. Residues 24 and 39 of MgTX are highlighted with bold lines.

history. In this alignment the sheet has an N-terminal extension of Ala^{25}, and a C-terminal extension of His^{39}, and is formed by considering which residues in the toxins occupy structurally similar positions in the β-sheet. An important feature of this alignment is that the residue corresponding to Arg^{25} in ChTX, which has been implicated in the interaction of ChTX with the high-conductance Ca^{2+}-activated K^+ channel (Park & Miller, 1992), is Gly^{26} in MgTX rather than Ala^{25} as indicated by the previous alignment.

One of the other significant differences between the sequence of MgTX and those of IbTX and ChTX is the presence in MgTX of two proline residues in a region analogous to the helix found in IbTX and ChTX. The refined structures of MgTX also have a helical conformation in this region, consistent with the observed NOEs and coupling constants. This is somewhat surprising in that proline residues are generally considered to have a very low probability of occurrence in helical regions because of the close contact that would occur between the δ-carbon of the proline and the β-carbon of the preceding residue. Based on energy modeling using ideal covalent bond lengths and angles, the calculated energy of the α-conformation of a residue preceding a proline is more than 7 kcal less favorable than the β-conformation (Schimmel & Flory, 1968; Summers & Karplus, 1990). Despite this consideration, approximately 9% of the non-Pro and non-Gly residues preceding proline residues are located in α-helical conformation (MacArthur & Thornton, 1991; Nicholson et al., 1992). When energy modeling is done using flexible geometries, the energy difference drops to 1.1 kcal/mol and the calculated energy surface is in excellent agreement with observed conformational distributions (Hurley et al., 1992). The expected occurrence of Pro-Pro sequences in helical regions is even lower due to the expected close contact between the δ-carbons of the adjacent proline residues. Of 37 examples of X-Pro-Pro-X sequences as found in 26 high-resolution (<2.5 Å) protein structures, there is one example (the third and fourth residues of the H helix in hemoglobin) that has both residues in the α conformation (MacArthur & Thornton, 1991). It is likely that in this example the expected close contact (between δ-carbons) is also relieved by alterations of bond angles and distances.

Consistent with the above is the fact that the highest energy nonbond contact observed in the MgTX structures generated with the rigid-geometry program PEGASUS is between the δ-carbons of proline 15 and 16. The average $C^\delta-C^\delta$ distance between these two residues is 2.4 Å, and the resulting contribution to the contact energy is approximately 25 kcal/mol. It is likely that in MgTX the close $C^\delta-C^\delta$ contact is relieved by compensating changes of the covalent bond angles and lengths of these residues from their canonical values. Indeed, when the structures are further refined with the flexible-geometry program X-PLOR (Brünger, 1991) the average $C^\delta-C^\delta$ distance increases to 2.9 Å. Furthermore, the strain induced by the presence of the Pro-Pro sequence in the helix is likely compensated by the disulfide bonds formed by Cys^{13} and Cys^{17} which bracket this sequence.

A possible role for this sequence is suggested by the work of Venkatachalapathi and Balaram (1979), who proposed that a Pro-Pro sequence could function as a helix nucleation site. They showed that NMR and IR spectra of a Piv-Pro-Pro-Ala-NHME peptide sequence are consistent with a 3_{10}-helical conformation. Thus, the Pro-Pro site in MgTX could function during protein folding by acting as an aid to helix nucleation. A favorable consequence of this would be to aid in orientation of the bracketing cysteine residues such that they are in appropriate positions to form the correct disulfide bonds to the two cysteines of the β-sheet.

Analysis of the effect of a large number of mutants of charybdotoxin on that toxin's interaction with a high-conductance Ca^{2+}-activated K^+ channel has allowed the elucidation of the interaction surface of the toxin (Stampe et al., 1994). This interaction surface consists of eight residues: Ser^{10}, Trp^{14}, Arg^{25}, Lys^{27}, Met^{29}, Asn^{30}, Arg^{34}, and Tyr^{37}. The latter six residues are all found on the antiparallel β-sheet. Lys^{27}, Met^{29}, Asn^{30}, and Tyr^{37} all occur in analogous positions in MgTX and Arg^{34} is conservatively replaced by Lys. The lack of an effect of the Ser10Gln mutant on ChTX on-rate with Shaker K^+ channel (Stampe et al., 1994) suggests that this region may not be important in binding to voltage-gated channels. The MgTX residue that is analogous in placement to Arg^{25} is Gly^{26}. Thus, assuming that the interaction surface of MgTX is largely formed by the β-sheet, the presence of an Arg at this position is not a key determinant of $Kv_{1.3}$ binding. Conversely, lack of this residue may play a key role in MgTX's lack of activity on large-conductance Ca^{2+}-activated K^+ channels. The role of the C-terminal domain of these toxins in determining channel selectivity is further supported by the study of IbTX-ChTX

and ChTX-IbTX chimeric peptides (Giangiacomo et al., 1993). In these peptides the C-terminal domain of ChTX defines the toxin−channel interactions that distinguish between the maxi-K channel and $Kv_{1.3}$.

An important determinant of specificity that is not apparent from single-residue mutagenesis of these toxins may be the longer β-sheet in MgTX. The model proposed for ChTX interaction with Ca^{2+}-activated K^+ channel has the toxin resting in a vestibule at the pore entrance. The wall of this vestibule is deduced from the analysis of the Ser^{10} and Trp^{14} mutants and is presumed to be about 7 Å high (Stampe et al., 1994). The interaction surface of ChTX extends the full length of the β-sheet as indicated by the presence of the key residues Arg^{25} and Asn^{30}. As noted above the additional two residues in MgTX extend the β-sheet by one residue relative to ChTX and IbTX. This may create a steric block that prevents the MgTX from properly fitting into the vestibule. Given the fact that analogs of MgTX can be readily made by both synthetic (Bednarek et al., 1994) and recombinant methods (Garcia-Calvo et al., 1993), these hypotheses can be tested directly. Such studies are in progress.

ACKNOWLEDGMENT

We acknowledge Dr. Reid J. Leonard for helpful discussions.

REFERENCES

Ausubel, F. M., Brent, R., Kingston, R. E., Moore, D. D., Seidman, J. G., Smith, J. A., & Struhl, K. (1989) *Current Protocols in Molecular Biology*, John Wiley & Sons, New York.

Barkhuijsen, H., De Beer, R., Bovée, W. M. M. J., & van Ormondt, D. (1985) *J. Magn. Reson. 61*, 465−481.

Bax, A., & Davis, D. G. (1985) *J. Magn. Reson. 63*, 207−213.

Bednarek, M. A., Bugianesi, R. M., Leonard, R. J., & Felix, J. P. (1994) *Biochem. Biophys. Res. Commun. 198*, 619−625.

Berstein, F. C., Koetzle, T. F., Williams, G. J. B., Meyer, E. F., Jr., Brice, M. D., Rodgers, J. R., Kennaard, O., Shimanouchi, T., & Tasumi, M. (1977) *J. Mol. Biol. 112*, 535−542.

Bontems, F., Roumestand, C., Boot, P., Gilquin, B., Doljansky, Y., Ménez, A., & Toma, F. (1991a) *Eur. J. Biochem. 196*, 19−28.

Bontems, F., Roumestand, C., Gilquin, B., Ménez, A., & Toma, F. (1991b) *Science 254*, 1521−1523.

Bontems, F., Gilquini, B., Roumestand, C., Menez, A., & Toma, F. (1992) *Biochemistry 31*, 7756−7764.

Bothner-By, A. A., Stephens, R. L., Lee, J.-M., Warren, C. D., & Jeanloz, R. W. (1984) *J. Am. Chem. Soc. 106*, 811−813.

Boucher, W., Laue, E. D., Campbell-Burk, S. L., & Domaille, P. J. (1992) *J. Biomol. NMR 2*, 631−637.

Braunschweiler, L., & Ernst, R. R. (1983) *J. Magn. Reson. 53*, 521−558.

Brooks, B. R., Bruccoleri, R. E., Olafson, B. D., States, D. J., Swaminathan, W., & Karplus, M. (1983) *J. Comput. Chem. 4*, 187−217.

Brünger, A. T. (1991) *X-PLOR. Version 3.1. A System for X-ray Crystallography and NMR*, Yale University Press, New Haven, CT.

Campbell-Burk, S. L., Domaille, P. J., Starovasnik, M. A., Boucher, W., & Laue, E. D. (1992) *J. Biomol. NMR 2*, 639−646.

Davis, D. G., & Bax, A. (1985) *J. Am. Chem. Soc. 107*, 2820−2821.

Deutsch, C., Price, M., Lee, S., King, V. K., & Garcia, M. L. (1991) *J. Biol. Chem. 266*, 3668−3674.

Driscoll, P. C., Clore, G. M., Beress, L., & Gronenborn, A. M. (1989) *Biochemistry 28*, 2178−2187.

Freedman, B. D., Price, M. A., & Deutsch, C. J. (1992) *J. Immunol. 49*, 3784−3794.

Garcia, M. L., Galvez, A., Garcia-Calvo, M., King, V. F., Vazquez, J., & Kaczorowski, G. J. (1991) *J. Bioenerg. Biomembr. 23*, 615−646.

Garcia-Calvo, M., Leonard, R. J., Novick, J., Stevens, S. P., Schmalhofer, W., Kaczorowski, G. J., & Garcia, M. L. (1993) *J. Biol. Chem. 268*, 18866−18874.

Giangiacomo, K. M., Sugg, E. E., Garcia-Calvo, M., Leonard, R. J., McManus, O. B., Kaczorowski, G. J., & Garcia, M. L. (1993) *Biochemistry 32*, 2363−2370.

Gimenez-Gallego, G., Navia, M. A., Reuben, J. P., Katz, G. M., Kaczorowski, G. J., & Garcia, M. L. (1988) *Proc. Natl. Acad. Sci. U.S.A. 85*, 3329−3333.

Griesinger, C., Sørensen, O. W., & Ernst, R. R. (1982) *J. Am. Chem. Soc. 104*, 6800−6802.

Grinstein, S., & Smith, J. D. (1990) *J. Gen. Physiol. 95*, 97−120.

Grzesiek, S., Ikura, Clore, G. M., Gronenborn, A. M., & Bax, A. (1992) *J. Magn. Reson. 96*, 215−221.

Güntert, P., Braun, W., Billeter, M., & Wüthrich, K. (1991a) *J. Am. Chem. Soc. 111*, 3997−4004.

Güntert, P., Braun, W., & Wüthrich, K. (1991b) *J. Mol. Biol. 217*, 517−530.

Hille, B. (1992) *Ionic Channels of Excitable Membranes*, Sinauer Associates, Inc., Sunderland, MA.

Hurley, J. H., Mason, D. A., & Matthews, B. W. (1992) *Biopolymers 32*, 1443−1446.

Johnson, B. A. (1992) *J. Magn. Reson. 100*, 189−194.

Johnson, B. A., & Sugg, E. E. (1992) *Biochemistry 31*, 8151−8159.

Johnson, B. A., & Blevins, R. A. (1994) *J. Biomol. NMR 4*, 603−614.

Kay, L. E., Clore, G. M., Bax, A., & Gronenborn, A. M. (1990) *Science 249*, 411−414.

Kim, Y., & Prestegard, J. H. (1989) *J. Magn. Reson. 84*, 9−13.

Leonard, R. J., Garcia, M. L., Slaughter, R. S., & Reuben, J. P. (1992) *Proc. Natl. Acad. Sci. U.S.A. 89*, 10094−10098.

Lin, C. S., Boltz, R. C., Blake, J. T., Nguyen, M., Talento, A., Fischer, P. A., Springer, M. S., Sigal, N. H., Slaughter, R. S., Garcia, M. L., Kaczorowski, G. J., & Koo, G. C. (1993) *J. Exp. Med. 177*, 637−645.

MacArthur, M. W., & Thornton, J. M. (1991) *J. Mol. Biol. 218*, 397−412.

MacKinnon, R., & Miller, C. (1988) *J. Gen. Physiol. 91*, 335−349.

Marion, D., Ikura, M., Tschudin, R., & Bax, A. (1989) *J. Magn. Reson. 85*, 393−399.

Nicholson, H., Tronrud, D. E., Becktel, W. J., & Matthews, B. W. (1992) *Biopolymers 32*, 1431−1441.

Nilges, M., Clore, G. M., & Gronenborn, A. M. (1990) *Biopolymers 29*, 813−822.

Park, C. S., & Miller, C. (1992) *Biochemistry 31*, 7749−7755.

Park, C. S., Hausdorff, S. F., & Miller, C. (1991) *Proc. Natl. Acad. Sci. U.S.A. 88*, 2046−2050.

Powers, R., Gronenborn, A. M., Clore, G. M., & Bax, A. J. (1991). *J. Magn. Reson. 94*, 209−213.

Price, M., Lee, S. C., & Deutsch, C. (1989) *Proc. Natl. Acad. Sci. U.S.A. 86*, 10171−10175.

Robson, B., & Platt, E. (1986) *J. Mol. Biol. 188*, 259−281.

Rosa Barros, M., Simon, V., & Rosenblatt, M. S. (1989) *Cell Biochem. Funct. 7*, 219−226.

Sands, S. B., Lewis, R. S., & Cahalan, M. D. (1989) *J. Gen. Physiol. 93*, 1061−1074.

Sanger, F., Nicklen, S., & Coulson, A. R. (1977) *Proc. Natl. Acad. Sci. U.S.A. 74*, 5463−5467.

Schimmel, P. R., & Flory, P. J. (1968) *J. Mol. Biol. 34*, 105−120.

Schmieder, P., Thanabal, V., McIntosh, L. P., Dahlquist, F. W., & Wagner, G. (1991) *J. Am. Chem. Soc. 113*, 6323−6324.

Sedmark, J. J., & Grossberg, S. E. (1977) *Anal. Biochem. 79*, 544−552.

Slaughter, R. S., Shevell, J. L., Felix, J., Lin, C. S., Sigal, N. H., & Kaczorowski, G. J. (1991) *Biophys. J. 59*, 213 (abstr.).

Smith, C., Phillips, M., & Miller, C. (1986) *J. Biol. Chem. 261*, 14607−14613.

Stampe, P., Kolmakova-Partensky, L., & Miller, C. (1994) *Biochemistry 33*, 443−450.

Studier, F. W., & Moffat, B. A. (1986) *J. Mol. Biol. 189*, 113−130.

Sugg, E. E., Garcia, M. L., Reuben, J. P., Patchet, A. A., & Kaczorowski, G. J. (1990) *J. Biol. Chem. 265*, 18745−18748.

Summers, N. L., & Karplus, M. (1990) *J. Mol. Biol. 216*, 991−1016.

Vazquez, J., Feigenbaum, P., Katz, G., King, V. F., Reuben, J. P., Slaughter, R. S., Kaczorowski, G. J., & Garcia, M. L. (1989) *J. Biol. Chem. 264*, 20902−20909.

Vazquez, J., Feigenbaum, P., King, V. F., Kaczorowski, G. J., & Garcia, M. L. (1990) *J. Biol. Chem. 265*, 15564−15571.

Venkatachalapathi, Y. V., & Balaram, P. (1979) *Nature 281*, 83−84.

Vuister, G. W., Delaglio, F., & Bax, A. (1992) *J. Am. Chem. Soc. 114*, 9674−9675.

Wüthrich, K. (1986) *NMR of Proteins and Nucleic Acids*, John Wiley & Sons, New York.